PHILOSOPHICAL TRANSACTIONS OF THE ROYAL SOCIETY A MATHEMATICAL, PHYSICAL & ENGINEERING SCIENCES

X-ray Spectroscopy of Laser Imploded Targets

B. Yaakobi, S. Skupsky, R. L. McCrory, C. F. Hooper, H. Deckman, P. Bourke and J. M. Soures

Phil. Trans. R. Soc. Lond. A 1981 **300**, 623-630
doi: 10.1098/rsta.1981.0090

Phil. Trans. R. Soc. Lond. A **300**, 623–630 (1981) [623]
Printed in Great Britain

X-ray spectroscopy of laser imploded targets

By B. Yaakobi, S. Skupsky, R. L. McCrory, C. F. Hooper,†
H. Deckman,‡ P. Bourke and J. M. Soures
Laboratory for Laser Energetics, University of Rochester, Rochester, New York 14623, *U.S.A.*

X-ray spectroscopy provides a variety of means for studying the interaction of lasers with plasmas, in particular the interaction with imploding targets in inertial confinement fusion. A typical fusion target is composed of materials other than the thermonuclear fuel which play a variety of roles (tamping, shielding, thermal isolation, etc.). These structural elements emit characteristic X-ray lines and continua, and through their spectral and spatial distributions can yield very valuable information on the interaction and implosion dynamics. Examples are the study of heat conductivity, the mixing of different target layers, and the determination of temperature and density at the compressed target core. Results will be shown for electron densities $N_e \approx 10^{24}$ cm^{-3} and temperatures $T \approx 1$ keV measured during compression of argon-filled targets with a six-beam laser of peak power 2 TW.

1. Introduction

X-ray spectroscopy of laser-produced plasmas has been extensively reviewed over the last few years (Bekefi *et al.* 1976, Peacock 1978, Key & Hutcheon 1980). Most of the past studies involved an arrangement where a single laser beam is focused on a flat target, and their interaction is investigated. Recently, with the advent of multi-beam lasers capable of symmetrically compressing spherical targets, a new field of measurement has opened up and new demands are made on experimental techniques and theory. The core of compressed targets can achieve an electron density N_e of order 10^{24} cm^{-3}, as compared with 10^{21} cm^{-3} in the laser absorption region. Reliable ways to measure such densities are required. The electron temperature in the compressed core is not much higher than can be achieved in the laser absorption region (up to 1–2 keV), although the ion temperature can be much higher. In addition to these parameters, the determination of the product ρR of the mass density and radius of the compressed core is crucial: it plays the same role as density multiplied by confinement time in magnetic confinement experiments. It also determines the onset of self-heating by absorption of thermonuclear reaction products (α particles).

Most of these parameters could be measured with nuclear particle methods if yields of these particles were much higher than can be achieved in most laser fusion experiments (through secondary nuclear reactions, nuclear activation of the target, etc.). X-ray spectroscopy, on the other hand, can provide direct measurement of electron temperature and density and of the ρR product for most current laser fusion experiments. For this to be feasible, the target should contain elements of sufficiently high nuclear charge Z to not be completely stripped of bound electrons, so that X-ray lines will appear in the spectrum. Inertial confinement targets do contain layers of such elements which perform a variety of important roles in the implosion dynamics. Radiation losses due to such 'impurities' are not as lethal as in magnetic confinement

† Permanent address: University of Florida, Gainesville, Florida 32611, U.S.A.
‡ On assignment from Exxon Research and Engineering Company, Linden, New Jersey, U.S.A.

devices because self-heating through α particle deposition would, under the right conditions, overcome these losses. Additionally, one can construct targets with the main purpose of maximizing the ability to diagnose the implosion dynamics rather than maximizing the nuclear yield.

As an example of such a procedure, we describe here the results of an experiment conducted recently at the Laboratory for Laser Energetics of the University of Rochester, where Argon-filled glass shells over-coated with plastic were imploded with the six-beam laser system Zeta (Bunkenburg & Seka 1979). In addition to being able to measure compressed core parameters, these experiments can provide information on such crucial questions as shell-fill mixing and preheat of the core by supra-thermal electrons. Mixing can arise because of hydrodynamic instability or lack of complete spherical symmetry. It carries the danger of aborting the compression before it peaks or allowing high-Z material to drift to the centre before it is ignited. Preheat is caused by long mean-free-path electrons produced at the critical layer, where the laser is mostly absorbed. Preheat prevents the target from compressing to a high density because compression at a higher temperature requires more energy.

The primary theoretical development needed for the successful implementation of X-ray spectroscopy is the calculation of Stark-broadened line profiles which are used for density determination. We use here profiles calculated by C. F. Hooper & L. A. Woltz (1979 unpublished technical report, Department of Energy Contract no. DE-ASOS-76DP40016, Department of Physics and Astronomy, University of Florida). Similar calculations have been made by Kepple & Griem (1979, private communication) and by Lee (1979*a*, *b*). Additional development may be required especially for the part of the profiles around the line centre and for the determination of possible line shifts due to plasma effects. Such shifts (and asymmetries) can be related through the potential in the plasma to the important question of the equation of state of dense matter.

An earlier account of part of this work is given in Yaakobi *et al.* (1980).

2. Argon-filled target implosions

Most current implosion experiments in laser fusion are directed toward the compression of targets to densities significantly higher than previously achieved (0.1–0.5 g/cm^3) in the so-called explosive-pusher régime. We report here on high compression experiments in which we used thick shell targets filled with argon and imploded with short, high intensity laser pulses. The role of the argon was two-fold: (i) partly to mitigate the effect of preheat through radiational cooling and thereby enable a higher compression; (ii) to serve as a direct diagnostic of the compressed density (ρ) and the quality of confinement (ρR). The relevance of these experiments to D–T-filled target implosions is that for a given mass density (or electron density) the compressed core pressure (due to both electrons and ions) in both cases will be comparable. More importantly, the measurement of the density (by using X-ray line Stark broadening) enables an experimental verification of whether a given predicted compression (with any fill) can be achieved or whether it is prevented by the lack of perfect spherical symmetry, instability or shell-fill mixing.

The calculation of the Stark profiles used here will be described in a forthcoming publication. Fitting these profiles to the observed lines involves methods similar to those used to interpret various neon-filled target experiments. The various lines are predicted to have different widths

and *very different shapes*, and therefore a consistent agreement with this large number of observables constitutes a highly reliable determination of the compression.

The experiments were conducted on the symmetrical irradiation, six-beam Nd-glass laser facility Zeta. X-ray spectra were measured with Ge ($2d = 0.65$ nm) and gypsum ($2d = 1.515$ nm) crystals, a slit being used for spectral imaging of resolution of *ca.* 11 μm. The film (Kodak 2497) was calibrated at a few wavelengths (recorded argon lines usually had a diffused density on film of less than 0.3 optical density for which film density is proportional to exposure). Typical data given in table 1 include three out of a series of thirty shots producing high density (i.e. thick shells) which showed similar and very consistent spectral results.

TABLE 1. PARAMETERS OF ARGON-FILLED TARGET IMPLOSIONS

shot no.	power TW	diameter μm	wall thickness μm	polymer coating μm	Ar-fill pressure atm†	Ar-Lyman-β width/eV measured	Ar-Lyman-β width/eV computed (LILAC)	inferred density g/cm³	inferred compression ratio
3231	1.8	52	1.86	1.58	16	46 ± 3	41	6.0 ± 1.5	250
2495	2.0	51	0.50	4.20	7	42 ± 3	39	5.2 ± 1.3	470
3264	2.0	50	1.90	1.88	< 3	43 ± 5	37	6.0 ± 2.0	> 1000
2416	1.7	45	0.48	1.60	8.7	20 ± 2	18	< 1.5	< 100

† atm = 101 325 Pa.

To employ the observed lines for ρ and ρR determinations we need to estimate the temperature during emission, and the opacity (self-absorption) of the lines. The core temperature needs to be known only approximately for Stark profile fitting, especially for helium-like ions. For example, in going from $T = 0.8$ keV to 1.2 keV, N_e being kept constant at $N_e = 10^{24}$ cm^{-3}, the width of the Ar^{16+}, $1s^2$–$1s3p$ line increases by less than 4%. The temperature also determines the Doppler broadening (*ca.* 1.5 eV); this and the instrumental width (*ca.* 1 eV) were included in the Stark profiles (although their effect is very small). For the high density shots, T_e was found to be about 0.8 keV by using various line intensity ratios. The optical depth at an energy distance ΔE from the centre of a spectral line depends on the line profile $S(\Delta E)$ through $\tau(\Delta E) \sim \rho R b\, S(\Delta E)$, where b is the population fraction of ions in the absorbing level. For Stark broadened lines the optical depth close to the line centre is approximately independent of the compressed density ρ, since $S \sim \rho^{-\frac{2}{3}}$ whereas $\rho R \sim \rho^{\frac{2}{3}}$. For example, the opacity at the peaks of the Ar^{17+} Lyman-β line is given by $\tau_m \approx 0.1\, bP^{\frac{1}{3}}R_0$, where P is the fill pressure (in atmospheres: atm = 101 325 Pa) and R_0 the initial radius (in micrometres). For one-electron ions $b \lesssim 0.4$ and we find for typical high density shots that $\tau_m \lesssim 1.5$ (or $\tau_0 \lesssim 0.5$ for the line centre). This means that Lyman-β lines can yield the density, but a small opacity correction may be required. For Lyman-γ lines the opacity is negligible whereas for Lyman-α lines we find $\tau_m = \tau_0 > 100$; these lines can therefore be used to give the ρR-value. For the $1s^2$–$1s3p$ line we find $\tau_0 \lesssim 2$ (here $b \lesssim 0.9$).

An example of density determination is shown in figure 1 for shot 3231. The Lyman-β line was fitted with a profile of electron density $N_e = (1.5 \pm 0.4) \times 10^{24}$ cm^{-3} (which corresponds to $\rho \approx 6$ g/cm³) without any opacity correction; a small correction would further improve the agreement with the experiment. The discrepancy around the line centre could be due to omission in the theory of additional broadening mechanisms as well as low-density contributions to the observed, integrated line profile; neither would significantly alter the rest of the

profile. The peak separation is relatively insensitive to opacity (or to background subtraction and corrections to the theory) and is very useful in obtaining a first estimate of the density.

Figure 1 shows that the profile shapes of argon lines agree with theory: Lyman-β is split in the centre whereas Lyman-γ has a sharp central peak. At the density deduced here the line $1s^2$–$1s4p$ should broaden until it is very similar to the Lyman-γ profile (transition from quadratic to linear Stark effect). This is indeed the case in figure 1 where the widths of these two lines (62 and 58 eV, respectively) compare well with the predicted f.w.h.m. of 64 eV for the Lyman-γ line at a density $N_e = 1.5 \times 10^{24}\ \mathrm{cm}^{-3}$.

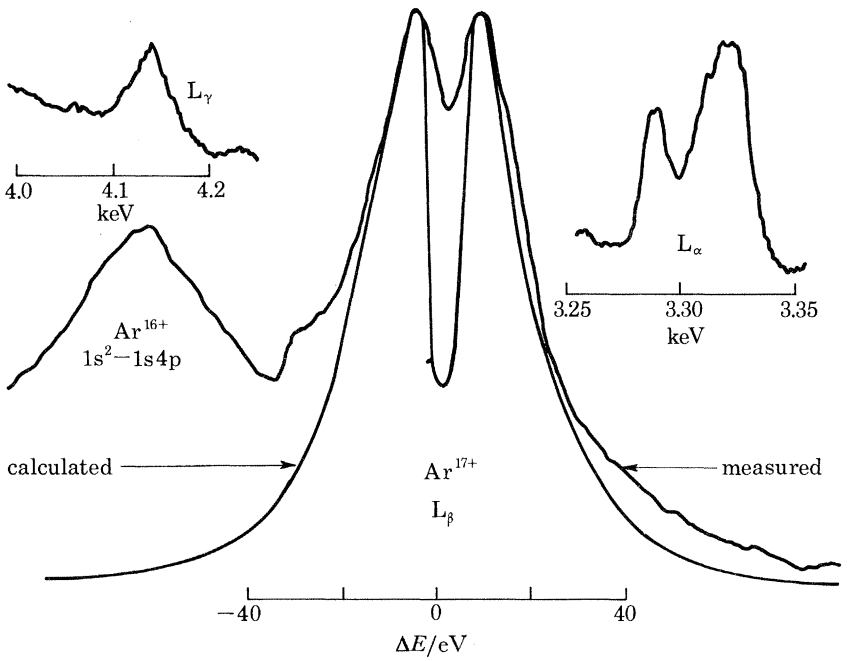

FIGURE 1. Argon lines from shot no. 3231 (target is quartz shell so neither K nor Ca appear in the spectrum). The theoretical Stark profile is calculated for $N_e = 1.5 \times 10^{24}\ \mathrm{cm}^{-3}$ or $\rho \approx 6\ \mathrm{g/cm}^3$. The inserts show the measured profiles of the Lyman-γ (L_γ) and Lyman-α (L_α) lines of Ar^{17+}.

Some of the more dramatic profile changes with density are shown by the spectral profile of the $1s^2$–$1s3p$ line of Ar^{16+} and its forbidden neighbour $1s^2$–$1s3d,3s$. Figure 2 shows a comparison of the profile of these lines for a high density shot (2495) and for a lower density shot (2416). At high plasma densities the quadratic Stark effect should cause the forbidden line to increase in intensity and the two lines to move apart and broaden. All these features are clearly seen in figure 2. Stark profile fitting (figure 3) yields an electron density $N_e = (0.96 \pm 0.24) \times 10^{24}\ \mathrm{cm}^{-3}$ ($\rho \approx 3.8\ \mathrm{g/cm}^3$). The Stark profile for this density has the correct peak separation but is too narrow; we then introduce opacity and increase it until good agreement with the experiment is achieved. The opacity correction *does not significantly change the peak separation*, and therefore the observed profile cannot be fitted with a profile corresponding to a lower density and higher opacity. The opacity needed for good agreement in figure 3 agrees with its estimated value (above). Also, the Lyman-β line corresponding to figure 3 was well fitted with a profile of density $N_e = 1.3 \times 10^{24}\ \mathrm{cm}^{-3}$ ($\rho \approx 5.2\ \mathrm{g/cm}^3$) after a small correction for opacity ($\tau_0 = 0.5$) had been included.

Stark profiles yield only the total electron (or mass) density in the emission region. However, the opacity-broadened Ar Lyman-α line yields the ρR for argon alone and can show whether the measured density corresponds to an argon–glass mixture. The Stark width of this line at the density deduced from the Lyman-β line would be smaller than the fine-structure splitting (4.7 eV). The observed additional broadening to a f.w.h.m. of 28 eV is due to opacity. At the

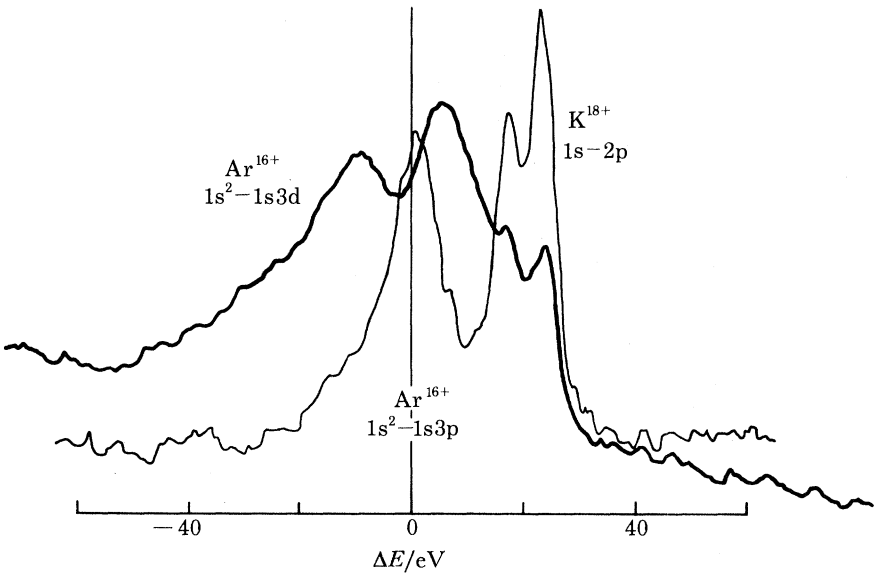

FIGURE 2. Argon lines from a thin uncoated (——) and from a coated target (——) (shot no. 2495). The quadratic Stark effect due to the high plasma density causes line shift, broadening and appearance of the normally forbidden $1s^2$–$1s3d$ line (including a contribution from the $1s^2$–$1s3s$ forbidden line).

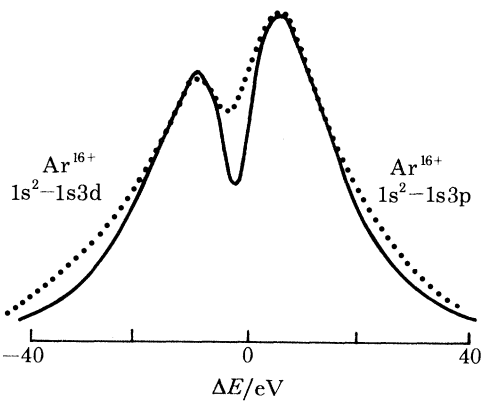

FIGURE 3. Density determination by fitting the observed lines in figure 2 (···) with a computed Stark profile (——). Note that the 3s level has a small contribution to the forbidden line and is included in the calculation. $N_e = 0.96 \times 10^{24}$ cm^{-3}; $\rho = 3.8$ g/cm^3; $T = 0.8$ keV, $\tau_0 = 1.0$.

half-intensity points $\tau \approx \ln 2$, and the value of the Stark profile at $\Delta E = 1$ eV for a density $N_e = 1.5 \times 10^{24}$ cm^{-3} is 3×10^{-3} eV^{-1}. Since $b \lesssim 0.4$ we find from the definition of τ that $\rho R \gtrsim 10^{-3}$ g/cm^2. For such large values of ΔE the profile is well known and is independent of the uncertainties as to the narrow (less than 2 eV) central Stark component. If we assume a uniform density of 6 g/cm^3 in a compressed argon sphere (which overestimates ρR) we obtain

$\rho R < 2 \times 10^{-3}$ g/cm^2. Thus, to within 30% we find $\rho R = 1.5 \times 10^{-3}$ g/cm^2, which is consistent with the assumption that the total initial argon mass is compressed. Targets with lower fill-pressures yielded about the same density but necessarily a higher compression ratio (more than 1000 for shot 3264). We can conclude from this shot that no more than about 3×10^{-10} g of glass could be mixed with the argon, as the Lyman-α line would then be measurably narrower.

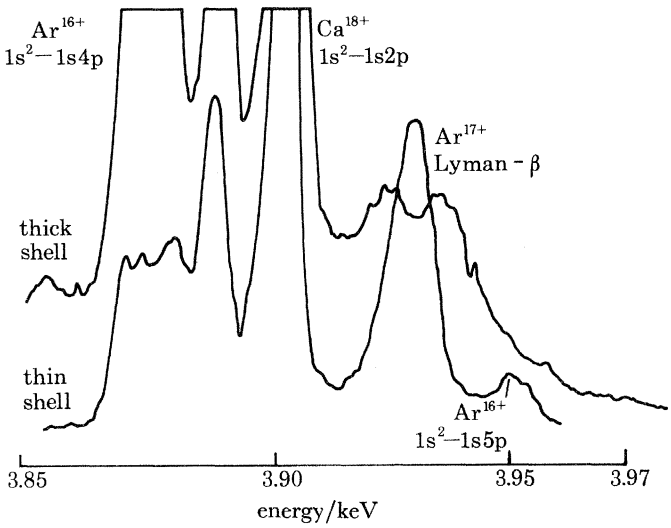

FIGURE 4. Evidence for higher compressed core density for a thicker shell implosion: the Ar^{17+} Lyman-β line becomes wider and acquires the characteristic shape of a Stark-broadened line.

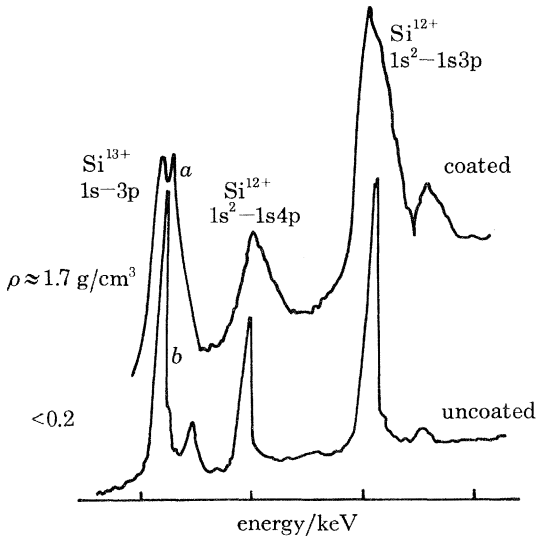

FIGURE 5. Silicon lines from shot 2495 (*a*) and a low compressed density shot for comparison (*b*). Note the broadening of the lines for the thicker shell, (*a*).

Figure 4 shows that the Ar^{17+} Lyman-β line is broad and has the characteristic Stark profile only for a thick shell implosion where theory predicts a higher density at peak compression.

In the high density implosions the inner part of the glass shell is recompressed to a moderately high density. In figure 5 we compare part of the silicon spectrum for shot 2495 with that of a low density shot. The broad lines are very similar in shape to the corresponding transitions in

argon: $1s^2$–$1s3p$ is blue-shifted (see figure 2), $1s^2$–$1s4p$ is centrally peaked and 1s–3p (of width 22 eV) is split in the centre. These Stark profiles yield a density of about 2 g/cm^3, which agrees with numerical predictions.

Figure 6 shows the spatial profiles of individual X-ray lines of the indicated ion species. The compression cannot be determined from these curves because the curve for argon is resolution limited; i.e., the size of the argon emission region consistent with the density derived above would be smaller than 11 μm. However, the curves of figure 6 do indicate the absence of strong mixing of glass material and fill gas during emission. This is shown by a computer simulation code (see below) to occur well after the shell starts to decelerate which is when instability leading to mixing could occur. Abel inversion applied to the chlorine and silicon curves produced shell-like emission profiles with peaks at the positions marked by the short vertical bars. For the calcium curve, insufficient resolution renders the Abel inversion impractical.

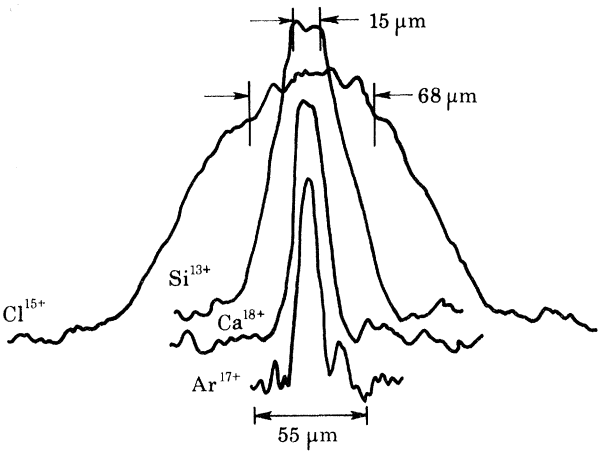

FIGURE 6. Spatial profiles of individual spectral lines of the indicated ion species (shot no. 2495); f.w.h.m./μm: Cl, 120; Si, 38; Ca, 16; Ar, 11. Chlorine is a constituent of the plastic coating.

The precision of the calculated Stark profiles away from the centre depends partly on that of the electric field distribution which had been shown by comparison with Monte-Carlo calculations to be better than 5%. Integration over time and space in the experiment results in the far profile wings being related to a higher density than the closer wings; in that sense our profile fitting constitutes a lower bound on the peak density. The main factors limiting the precision are the opacity and the background subtraction. By varying these parameters we could estimate a precision of 25% in the determined density.

Extensive simulations of radiationally cooled targets, including these experiments, were done by using the one-dimensional laser fusion code LILAC and will be reported separately. The simulations show that Ar^{17+} lines are emitted mostly during a time interval of about 10 ps when the average fill density is about 5–6 g/cm^3 and the temperature about 0.8 keV. This explains why spectral line profiles from the code, transported through the target and self-consistently tied to an atomic rate-dependent model, agreed quite closely with Stark profiles calculated for a single density (as well as with the experiment, see table 1).

In conclusion, an example has been shown of the use of X-ray spectroscopy for the study of high density laser-irradiated target implosions. Among the many other relevant examples

which are outside the scope of this presentation we mention two: (i) the observation of self-absorbed (or self-reversed) X-ray lines; these are indicative of temperature gradients in the target and are related to the important question of the transport of suprathermal electrons, leading to preheat; and (ii) the use of multi-layered targets for the study of electron transport and implosion stability. Many experiments in this area which have contributed greatly to our understanding of target implosion have been performed elsewhere, notably at the Rutherford Laboratory Central Laser Facility. It seems that X-ray spectroscopy may play an ever increasing role in studying the more elaborate and structured targets now envisaged for successful laser fusion experiments.

This work was partially supported by the following sponsors: Exxon Research and Engineering Company, General Electric Company, Northeast Utilities Service Company, The Standard Oil Company (Ohio, Sohio), and Empire State Electric Energy Research Corporation. Such support does not imply endorsement of the content by any of the above parties.

References (Yaakobi *et al.*)

Bekefi, G., Deutsch, C. & Yaakobi, B. 1976 In *Principles of laser plasmas* (ed. G. Bekefi), pp. 549–669. New York: John Wiley.

Bunkenburg, J. & Seka, W. 1979 In *Digest of technical papers, IEEE Conference on Laser Engineering and Application*, p. 96. New York: Institute of Electrical and Electronics Engineers.

Key, M. H. & Hutcheon, R. J. 1980 *Adv. atom. molec. Phys.* (In the press.)

Lee, R. 1979*a* *J. Phys.* B **12**, 1129–1143; ibid, 3445–3453.

Lee, R. 1979*b* *J. Phys.* B **12**, 3445–3453.

Peacock, N. J. 1979 In *Diagnostics for fusion experiments* (ed. E. Sindoni & C. Wharton), pp. 149–168. Oxford and New York: Pergamon.

Yaakobi, B., Skupsky, S., McCrory, R. L., Hooper, C. F., Deckman, H., Bourke, P. & Soures, J. M. 1980 *Phys. Rev. Lett.* **44**, 1072–1075.

PHILOSOPHICAL TRANSACTIONS OF THE ROYAL SOCIETY A MATHEMATICAL, PHYSICAL & ENGINEERING SCIENCES